Investigating effective strategies for sustainable operation of a submerged anaerobic membrane bioreactor (SAnMBR) coupled with ceramic ultrafiltration membrane

Chemical Engineering Journal 491 (2024) 151972

Contents lists available at ScienceDirect

Chemical Engineering Journal

journal homepage: www.elsevier.com/locate/cej

Investigating effective strategies for sustainable operation of a submerged anaerobic membrane bioreactor (SAnMBR) coupled with ceramic ultrafiltration membrane

Rajneesh Kumar Gautam [a], Akangbe Olubukola [b,c], Saumya Verma [d], Shobha Muthukumaran [a], Dimuth Navaratna [a,e,*]

[a] Institute for Sustainable Industries & Liveable Cities, College of Engineering and Science, Victoria University, Melbourne, VIC 3011, Australia
[b] School of Agriculture and Environment, Department of Environmental Sciences, University of Western Australia, Perth, WA, 6009
[c] Centre for Environment, Commonwealth Scientific and Industrial Research Organization, Western Australia, Perth, 6014
[d] Department of Innovation, Development and Information Technology, Community Broker Network, Melbourne, VIC, 3000, Australia
[e] ITCGU, Faculty of Engineering, University of Peradeniya, Prof. E. O. E. Pereira Mawatha, Kandy 20000, Sri Lanka

ARTICLE INFO

Keywords:
Critical Flux
Submerged AnMBR
Ultrafiltration
Cake Layer Biofouling
Biogas Sparging
Inorganic Fouling

ABSTRACT

This study presents a mechanistic approach to explore the key operational parameters governing the flux performance of an SAnMBR system coupled with a ceramic flat-sheet ultrafiltration membrane. Experiments were conducted at mixed liquor suspended solid (MLSS) concentrations of 12, 18, and 24 g/L using biogas sparging, backwashing, and a combination of both to investigate the most effective fouling mitigation strategy by exploring the fouling mechanism at a critical flux regime. To validate the experimental findings, a mathematical model was used to simulate the time-based variation of membrane effective pore radius (m), decrease in membrane porosity (%), thickness of cake layer (m), and membrane resistance (1/m). The study found that at a low biomass concentration, there was a sharp decline in the membrane pore radius leading to an increase in membrane resistance in the absence of any fouling mitigation strategies. However, by implementing these strategies individually and in combination, they maintained a higher pore radius and controlled the increase in membrane resistance even at high biomass concentrations. It was observed that biogas sparging outperformed the conventional backwashing strategy and the SAnMBR system exhibited superior performance attaining higher flux rates for prolonged duration. The advanced spectroscopic analysis confirmed the presence of a higher concentration of polysaccharides responsible for cake layer biofouling, and significant pore blocking due to inorganic foulants at high biomass concentrations. This suggests that the SAnMBR system must be operated at optimised biomass levels below the critical flux for sustained operation. Additionally, the key operational parameters identified using the mathematical model provide a precise assessment of SAnMBR performance, to improve its design efficiency for field applications.

Nomenclature

Symbol	Description (Unit)
n	Cake compressibility factor (−)
$\in_c$	Cake porosity (%)
C_b	Concentration of fouling particles in the bulk liquid (mg/L)
C_m	Concentration of fouling particles on the membrane surface (mg/L)
ϱ_c	Density of cake layer (kg/m^2)
X	Depth of cake layer ((m))

(*continued on next column*)

Nomenclature (*continued*)

d_p	Effective mean diameter of cake layer foulants (m)
K	First-order particle removal coefficient (kg/m^3.min)
J	Flux (L/m^2/h (LMH))
β	Gas sparging dependence coefficient (−)
K_v	gas sparging scouring coefficient. (kg. min/m^3)
r	Initial membrane effective Pore radius (nm)
f	Initial membrane porosity (%)
R_m	Intrinsic membrane resistance (1/m)

(*continued on next page*)

* Corresponding author at: Institute for Sustainable Industries & Liveable Cities, College of Engineering and Science, Victoria University, Melbourne, VIC 3011, Australia.
E-mail address: dimuth.navaratna@vu.edu.au (D. Navaratna).

https://doi.org/10.1016/j.cej.2024.151972
Received 10 January 2024; Received in revised form 8 April 2024; Accepted 5 May 2024
Available online 6 May 2024

Nomenclature (*continued*)

α_p	is membrane pore reduction coefficient ((m^3/mg))
δm	Membrane effective thickness (μm)
α_f	membrane porosity reduction coefficient ((m^2/mg),)
$\ddot{R}_C$	Membrane specific Resistance (1/m.kg)
P_c	Pressure drops across the cake layer (Pa)
R_c	Resistance due to cake layer (1/m)
R_p	Resistance due to pore blockage (1/m)
T	Time (d)
θ	Tortuosity (−)
R_t	Total filtration resistance (1/m)
TMP	Transmembrane pressure (kPa)
M	Viscosity of permeate (Pa.s)

1. Introduction

In recent years, there has been a remarkable increase in the adoption and application of anaerobic membrane bioreactors (AnMBRs) for treating high-strength industrial wastewater. Though advanced membrane bioreactor systems can operate in aerobic and anaerobic conditions, the latter provides significant benefits. These include energy generation in the form of biogas and a reduction in sludge yield [1]. The AnMBR system offers a practical solution when biomass granulation is not achievable or when a less turbid effluent, free of suspended solids and pathogens, is required. Previous studies have endorsed the multiple advantages of AnMBR systems, such as complete biomass retention irrespective of the microbial cell's biofilm or granule formation capability [2,3], superior effluent quality [4], improved disinfection potential [5], and reduced energy and space footprints [6].

Based on the previous research outcomes, it was evident that AnMBRs performed effectively in treating wastewater even under challenging conditions, including high organic loading, high salinity levels, elevated concentrations of suspended solids and particulate matter, and insufficient biomass granulation [7]. Despite these advantages, membrane fouling remains the primary hindrance to the widespread application of this innovative technology in treating industry wastewater containing high organics [8]. Fouling of membrane decreases permeate flux or increases *trans*-membrane pressure (TMP), leading to higher energy demand and operational costs [9,10]. Generally, the propensity of fouling of the membrane impacts the organic loading rate (OLR) and the biomass concentration, mainly measured as the bioreactor's mixed liquor suspended solid concentrations (MLSS).

Fouling could be irreversible or reversible depending on the mode of formation. Polymeric substances such as extracellular polymeric substances (EPS) are the major cause of reversible fouling which forms a cake layer on the surface of the membrane. In contrast, the soluble microbial products (SMP) are the key foulants present in the biomass which reduces the functional matrix of the membrane pores. These foulants can accumulate on the membrane surface and within the pores, causing cake layer formation and pore-blocking, respectively, and these occurrences considerably impact the biomass separation process [2]. The former refers to an intricate amalgamation of polysaccharides, proteins, lipids, and nucleic acids, creating a gel-like matrix with high hydration levels [11,12]. It is well established that these polymeric substances (EPS and SMP) at high biomass concentrations impart a significant obstacle to membrane filtration. They can significantly increase internal membrane fouling, up to six to seven times greater, and enhance membrane cake-layer formation [13].

The fouling of the membrane can be mitigated by optimizing the operating conditions and employing physicochemical cleaning methods [2]. Managing the flux through the membrane at a sustainable rate or operating below the critical flux, termed subcritical flux, will minimize the frequency of chemical cleaning due to excessive membrane fouling. The critical flux can also be considered a threshold value beyond which fouling becomes a significant issue. In an AnMBR system, the concept of critical time is related to the critical flux and plays a crucial role in determining the optimal operating conditions for the system. The critical time, in the context of AnMBR systems, refers to the time it takes for the critical flux conditions to be reached; at this point, fouling becomes significant and starts impacting the system's performance.

Operating an AnMBR system above the critical flux can lead to severe membrane fouling, emphasizing the importance of maintaining the operation below the critical flux (subcritical flux) [14]. The critical flux in the AnMBR system is influenced by various factors, including the bioreactor configuration, membrane characteristics, sludge properties, and operating conditions [15]. Several strategies have been suggested to limit flux decline, and they include intermittent and continuous biogas sparging [16], intermitted filtration modes, regulation of backwashing cycles and flux rates [17], and operating the process below the estimated critical flux [13]. Furthermore, considerable progress has been made in developing novel membrane types, such as ceramic ultrafiltration membranes with improved hydrophobicity and surface properties, to achieve higher flux rates with low fouling propensities and decrease their associated high costs [18].

Numerous recent studies have been conducted to understand the membrane fouling mechanisms and the flux regime of AnMBRs [4,7,10,16–20]. However, there is a noticeable absence of systematic investigation into the key factors influencing the critical flux of a submerged AnMBR system (SAnMBR), especially when treating a challenging industry effluent like abattoir wastewater [19,20]. Additionally, no study has been conducted to systematically investigate the impact of fouling mitigation strategies such as biogas sparging, traditional backwashing, and their combination (biogas sparging and backwashing) on the critical flux and time of an SAnMBR system coupled with a flat sheet ceramic ultrafiltration (UF) membrane to treat abattoir wastewater. In this context, this study presents a comprehensive investigation to identify the key parameters that govern the critical flux of a SAnMBR system incorporating continuous biogas sparging, backwashing, and a combination of both, aiming to identify the most effective fouling mitigation technique to attain higher flux rates. In addition, this study contributes significantly to understanding the correlations between key operational parameters and their optimisation for a sustainable SAnMBR operation.

2. Methodology

2.1. Experimental setup

The experimental setup of the SAnMBR system for conducting the critical flux tests (CFTs) is depicted in Fig. 1. The setup consisted of a water-jacketed, continually agitated glass fermenter (bioreactor) vessel with a 5 L hydraulic capacity. This setup was controlled using a BIOSTAT® automated controller (Applikon Bio Console ADI 1035). Polyvinyl Chloride (PVC) feed and permeate containers with 5 L and 50 L capacities were used to feed and collect treated permeate, respectively. The feed flow rate was controlled using a level sensor immersed in the bioreactor and interfaced with the BIOSTAT® to take signals and trigger the submersible pump to deliver more feed in the SAnMBR system. The characteristics of the ceramic ultrafiltration flat-sheet membrane module (GuoTech, Xiamen) are shown in Table 1. A peristaltic precision pump (Masterflex L/s 07551–20) connected with the membrane was used for collecting the high-quality treated permeate. After each set of critical flux experiments, the membrane module was removed from the bioreactor for cleaning and analysis purposes, and the SAnMBR was purged with N_2 gas (0.2 L/min for 5 min) to maintain strict anaerobic conditions. The temperature was maintained at 35 ± 2.5 °C by circulating hot water through the double wall glass fermenter from the hot-water bath connected to the bioreactor.

Two automatic electronically driven acid (0.1 M HCl) and base (0.1 M NaOH) dosing pumps were used to maintain the desired pH level in the bioreactor by injecting acid or base solutions into the system as needed. The membrane module was thoroughly cleaned before each critical flux test (CFT). Ex-situ chemical cleaning of the membranes was

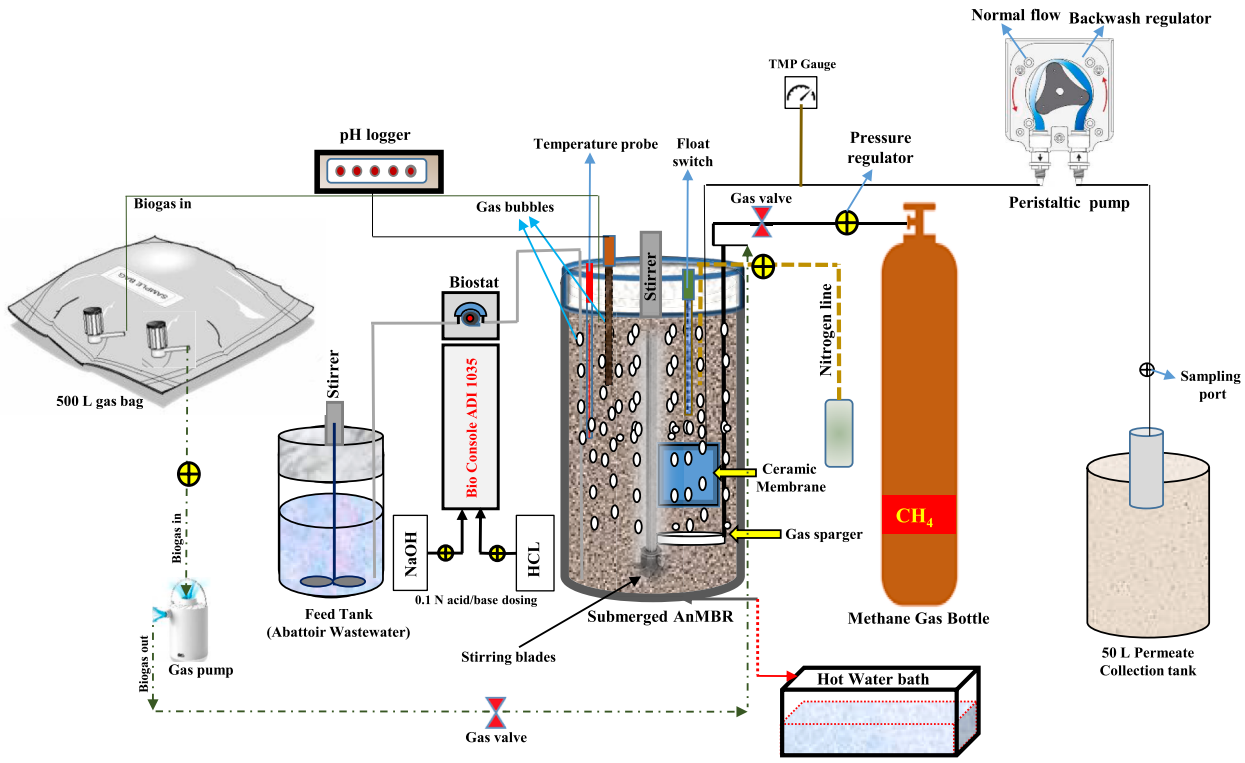

Fig. 1. A schematic of submerged AnMBR (SAnMBR) experimental setup.

Table 1
Characteristics of the ceramic flat sheet ultrafiltration membrane.

Parameter	Values
Material	Al_2O_3
Filtration mode	out-in
Module outer surface dimension (L*B*H) (m)	0.117 * 0.015 * 0.126
Module active surface dimension (L*B*H) (m)	0.086 * 0.006 * 0.110
Active membrane area (m^2)	0.02
Nominal pore size (μm)	0.1
Permeability ($L/m^2*h*bar$)	3300
Particle removal (nm)	≥ 100
Surface characteristics	Hydrophobic
Biogas sparging rate (L/min)	0.4

performed by soaking in 0.5 wt% (3 g/L NaOCl) hypochlorite following the protocol mentioned by [21]. Subsequent to this chemical cleaning process, about 300 ml of MiliQ ultrapure water was used to backwash the membrane at a negative TMP of 50 – 75 Pa for 5 – 7 min to remove residual NaOCl before immersing it in the SAnMBR [22]. The biogas produced by the SAnMBR was collected into a 500 L Polypropylene gas collection bag. A lab-scale mini dual-function pump (ScienceEqip) connected to a gas bag was used to sparge biogas into the bioreactor during the CFTs at a rate of 0.4 L/min. Since the collected biogas quantity was insufficient to complete all phases of CFTs, a high-purity methane gas bottle (Air Liquide Australia) was also used for gas sparging and completing the CFTs. The gas was pumped at a rate of 0.4 L/min to the perforated PVC circular manifold with approximately 15 holes (1.5 mm dia) installed at the base of the ceramic membrane module via valves, gas regulators and airflow metre.

2.2. SAnMBR operation

The CFT was conducted at 24 g/L, followed by 18 and 12 g/L. A sludge volume of around 50 ml was removed from the bioreactor after conducting the first set of critical flux experiments at 24 g/L, and a two-week gap was maintained for SAnMBR to achieve the designed MLSS concentrations of 18 and 12 g/L, respectively, to conduct subsequent sets of critical flux experiments. The synthetic abattoir wastewater was prepared according to the recipe described by [10] to feed the bioreactor during the CFT. The abattoir wastewater had a COD of 8300 ± 300 mg/L.

2.3. Experimental methods

2.3.1. Clean water membrane resistance test

A new ceramic UF membrane was used to conduct the clean water flux test for a baseline reference and improved equipment calibration following the method described [17]. A detailed methodology for conducting the clean water membrane resistance test is outlined in S.1 (Supplementary information).

2.3.2. Common flux-step critical flux test

The Critical flux was determined in this study using a common-flux step technique by Le Clech, Jefferson [23] and Bacchin, Aimar [24] at a flux step height of 1 LMH and step length of 15 min. A biogas sparging rate of 0.4 L/min was used in this study based on studies suggesting that this rate (0.4 L/min) can optimize mass transfer efficiency by enhancing the contact between biogas and the sludge in the SAnMBR system [16,25]. The CFTs were conducted at 12, 18 and 24 g/L MLSS concentrations in triplicates using four filtration modes: a) with no gas sparging and no backwashing, b) with gas sparging only, c) with backwashing only, and d) combined gas sparging and backwashing. Samples were collected at each flux step and stored for further analysis. The flux (J) and TMP were recorded at each flux step during the CFT experiment conducted at various biomass conditions using various fouling mitigation strategies, as discussed above.

2.3.3. Estimation of critical flux and time

The critical flux and critical time estimation were conducted through a graphical method [26–28]. The flux (J) and TMP were recorded at each flux step during the CFT experiments. This data was then plotted on a graph, with flux on the x-axis and TMP on the y-axis. The critical flux

was identified at the point where a visible change in the slope of the TMP vs. flux curve occurred, or a visible increase in TMP was observed [28], signifying a transition from a regime dominated by reversible fouling to one where irreversible fouling becomes significant. The slope representing a sharp increase in TMP was calculated using a polynomial regression model [29–31] of order three using a curve fitting function ("curve_fit") from the "scipy.optimize" module in Python software. The corresponding time at this transition point was marked as the critical time. A detailed explanation is summarized in S.2 (Supplementary information).

2.4. Analytical methods

The MLSS and MLVSS concentrations of bioreactor sludge samples were analysed using American Public Health Association (APHA): standard methods for the examination of water and wastewater [32,33].

2.4.1. Morphological analyses

Field Emission Scanning Electron Microscopy (FESEM) — Energy Dispersive Xray (EDX) and Nuclear Magnetic Resonance (NMR): A thorough examination was carried out using FESEM-EDX spectroscopic analysis to investigate the characteristics and concentrations of the foulants in the pore and surface of the membrane. Additionally, the SAnMBR sludge samples were collected during the CFT and were analysed in NMR to identify high molecular compounds, proteins and carbohydrates in the sludge samples following the procedure described by [34]. A detailed explanation is outlined in S.3 (Supplementary information).

2.5. Descriptive mathematical modelling

The mathematical expressions were used to simulate the time-based variation of membrane effective pore radius (m), decrease in membrane porosity (%), the thickness of cake layer (m) and membrane resistance (1/m) to understand the fouling mechanism and critical flux regime. The key parameters used in this modelling study are defined and listed in the nomenclature. Individual parameters and mathematical expressions are discussed comprehensively in the following sections (Section 2.5.1 – 2.5.5).

2.5.1. Flux

The flux can be expressed according to Darcy's law as,

$$J = \frac{TMP}{\mu R_t} \tag{1}$$

J is the permeate flux L/m^2/h (LMH), μ is permeate viscosity (kPa/day), and R_t is the total filtration resistance (1/m). The total resistance is the summation of the contribution of membrane resistance (R_m), resistance due to the cake layer (R_c), and resistance due to pore blockage (R_p).

$$R_t = R_m + R_p + R_c \tag{2}$$

Therefore, the flux becomes.

$$J = \frac{\Delta P}{\mu(R_m + R_p + R_c)} \tag{3}$$

It is assumed that during the beginning of the experiment, the R_p and R_c were zero.

2.5.2. Membrane intrinsic resistance

During the subcritical condition, fouling occurs due to the adsorption of soluble substances on the pores of the membrane surface, thereby increasing membrane intrinsic resistance. The membrane intrinsic resistance can be evaluated using the following empirical model (Eq. (4) given by [35].

$$R_m = \frac{8\theta\delta m}{fr^2_{pore}} \tag{4}$$

where θ is known as the membrane pore tortuosity, δm is membrane effective thickness (m), f is the decrease in membrane porosity (fraction of pore area) (%), r_{pore} is the membrane effective pore radius (m). Following the model proposed by [35], two differential equations were derived (Eqs. (5) and (6) to describe the adsorption of small particles within the membrane pores. The adsorption of small particles into the pores was described in terms of porosity reduction (Eq. (5) and the reduction of pore radius (Eq. (6)).

$$\frac{df}{dt} = -\alpha_f C_m J \tag{5}$$

$$\frac{dr_{pore}}{dt} = -\alpha_p C_m J \tag{6}$$

where α_f represents membrane porosity reduction coefficient (m^2/mg), α_p represents membrane pore reduction coefficient in (m^3/mg), C_m represents the concentration of fouling particles on the membrane surface (mg/L). Within the subcritical flux, there is no concentration polarization on the membrane surface; therefore, fouling is primarily due to small particle blockage of the membrane pores, and the concentration of particles within the subcritical region is the same as the concentration of foulants particles as it was contained in the bulk liquid [35].

In the supercritical region, there is a significant concentration polarization of the membrane surface due to the foulants particles; as a result, the cake layer acts as a precoat to tiny particles clogging the pores. Therefore, the concentration of smaller particles in the membrane pores is lower than in the bulk liquid.

2.5.3. Cake formation during the supercritical flux regime

Giraldo and LeChevallier [35] reported that the formation of a cake layer during the membrane filtration within the supercritical regime can be explained by the forward transport of floc particles from the bulk liquid to the membrane surface and the backward transport due to gas scouring. In this research, the scouring effect due to biogas sparging was considered.

The model was modified to suit this study and is expressed as,

$$\rho_c \frac{dx}{dt} = JC_b - K_v {V_{gas}}^{\beta} \tag{7}$$

where K_v represents the gas sparging scouring coefficient (mg/m^3), and V_{gas} represents the biogas sparging velocity (m/sec), x represents the thickness of the cake layer (m),C_b represents the concentration of cake particles in the bulk liquid (mg/L), β represents the gas sparging coefficient, and ρ_c represents the density of the cake layer (kg/m^3).

Eq. (7) represents the forward transport of foulants particles from the SAnMBR bulk liquid to the surface of the membrane and the backward transport of cake particles due to the biogas sparging.

2.5.4. Cake formation during the subcritical flux regime

The internal intrinsic membrane resistance is responsible for fouling within the subcritical flux regime, while external cake resistance and internal pore blockage are responsible during the supercritical flux regime [28]. The cake resistance during the subcritical flux conditions can be expressed as,

$$R_C = \ddot{R_C} x \tag{8}$$

where $\ddot{R_C}$ represents the cake layer-specific resistance (1/m^2), R_C represents the cake resistance (1/m), and x represents the thickness of the cake layer (m), as given in Eq. (7).

The famous Carman Kozeny equation [36] was used to evaluate the specific cake resistance and is expressed as,

$$\ddot{R}_C = \frac{180(1-\in_c)}{d^2{}_p \in_c{}^2} \quad (9)$$

where $\in_c$ represents cake porosity and d_p represents the effective mean diameter of the foulant cake particles (m). The effect of compressibility on the specific resistance of the cake layer can be expressed as,

$$\vec{R}_C = \ddot{R}_C P_c{}^n \quad (10)$$

where $\vec{R}_C$ represents the compressible specific cake resistance (1/m), P_C represents the pressure drops across the cake layer, and n represents the cake compressibility factor.

2.5.5. Kinetics of cake formation during supercritical flux regime

According to [35], cake formation follows first-order kinetics and is expressed as,

$$\frac{dC}{dt} = J\frac{dC}{dt} - kC \quad (11)$$

If $\frac{dC}{dt} = 0$, then

$$0 = J\frac{dC}{dt} - kC \quad (12)$$

By integration

$$C_m = C_b e^{\frac{kx}{J}} \quad (13)$$

where C_m represents the concentration of the foulant particle on the membrane surface (mg/L), C_b represents the concentration of the foulant particle in the SAnMBR bulk liquid (mg/L), and k represents the first-order particle removal coefficient. The model Equations (Eqs. (3), (4), (6), (7), and (13)) were simulated in Microsoft Excel Solver using the fixed parameter values taken from the literature, as shown in Table 2.

2.6. Data analysis and validation using statistical tools

A comprehensive statistical analysis was conducted to analyze the experimental dataset to investigate the influence of various fouling mitigation strategies at a given biomass concentration on critical flux and time. The statistical analysis included correlation and regression analysis and heat map generation. The correlation analysis was conducted to calculate the correlation coefficients between variables (flux and TMP) under different MLSS conditions; regression analysis, on the other hand, was conducted to quantify the relationship between these variables. A heat map was generated to visually represent the correlation matrix (S.4, Supplementary information), illustrating the relationships between flux and TMP across various MLSS concentrations. Furthermore, a linear model and polynomial regression model of order three were used to fit with the experimental data to estimate the key parameters. To compare the performance and suitability of these models, residual analysis and model comparison using statistical metrics such as R^2, mean absolute error (MAE) and mean squared error (MSE) were performed in Python software (v 3.11.4).

Table 2
Model input parameters.

Parameters	Symbols and Unit	Value	Reference
Density of cake layer	ρ_c ($\frac{kg}{m^2}$)	10^3	[59]
Initial membrane effective pore radius	r (nm)	3.5	[60]
Initial membrane porosity	f (%)	3.5	[60]
Gas sparging dependence coefficient	β(No unit)	1	[61]
Gas sparging scouring coefficient	K_v($\frac{kg.\,min}{m^3}$)	1.1 x 10^{-3}	[59]
Tortuosity	θ(No unit)	3.5	[62]
Membrane specific resistance	$\ddot{R}_C$ (m^{-1}/kg)	2 – 5 x 10^{12}	[63]
First-order particle removal coefficient	K (kg/m^3.min)	38.4 x 10^{-3}	[59]
Membrane effective thickness	δm(μm)	2.7	[60]

3. Results and discussion

The critical flux experiments demonstrated significant insights into the influence of biomass (MLSS) concentrations on the critical flux of a ceramic ultrafiltration (UF) membrane and the effectiveness of various fouling mitigation strategies for a sustainable SAnMBR operation. The critical parameters, including r (m), f (%), R_m (1/m), α_f (m^2/mg), and α_p (m^3/mg), were calculated for the new membrane for baseline reference using clean water flux tests (S1, Supplementary information) and compared for each biomass condition and fouling mitigation strategies and are discussed comprehensively in the subsequent sections.

3.1. Influence of biomass (MLSS) concentration on the critical flux of a SAnMBR system

For an MLSS concentration of 12 g/L, the critical flux of a SAnMBR system treating abattoir wastewater was determined at 7.05 LMH, whereas for 18 g/L, it decreased by 25.53 %, reaching 5.25 LMH. At 24 g/L, TMP reached the lowest flux of 4.35 LMH, showing a further 17.15 % decline in flux. Quantifying critical flux at MLSS of 12, 18, and 24 g/L reveals a systematic decline with increasing MLSS concentration, indicating a clear impact of biomass concentration on membrane fouling, as shown in Table 3 and Fig. 2(a). The temporal analysis of flux beyond specific critical values (7.05, 5.25, and 4.35) LMH highlights the onset of severe fouling, necessitating timely membrane cleaning or fouling mitigation strategies. This observation was in agreement with literature findings that higher biomass leads to increased membrane fouling due to more significant particle deposition on the surface of the membrane [15,37], while the analysis of TMP vs Flux slope provides a quantitative measure of fouling propensity. The TMP vs flux slope was also steeper for higher MLSS concentrations (18 and 24 g/L), reflecting a more rapid increase in TMP and, thus, a higher fouling propensity, as shown in Fig. 2(a) during no backwashing or biogas sparging condition.

Comparative references to existing literature strengthen these findings, as reported in a previous study, Giraldo and LeChevallier [35] stipulated a sharp decrease in critical flux as the concentration of biomass increases, corresponding to a decrease from 140 LMH to about 47 LMH when the biomass concentration increased from 0.4 g/L to 2 g/L. Moreover, Yuliwati, Ismail [38] also reported a decrease in critical flux with an increase in MLSS concentration, which resulted from increased concentration polarization due to the rising biomass concentration on the membrane's surface. Overall, the MLSS concentration plays a critical role in determining the flux behaviour of SAnMBR systems. By controlling the MLSS concentrations, implementing fouling mitigation strategies, and optimizing operating conditions such as hydraulic retention time (HRT) and solids retention time (SRT), the SAnMBR system can attain higher critical flux, leading to more efficient and sustainable SAnMBR operation.

3.2. Impact of biogas sparging on the critical flux

To evaluate the impact of biogas sparging on critical flux, the SAnMBR system was operated with biogas sparging at a flow rate of 0.4 L/min. The addition of biogas sparging resulted in a substantial increase in critical flux with a 72.34 % increase, from 7.05 LMH (no sparging or backwashing) to 12.5 LMH when operated with sparging at an MLSS concentration of 12 g/L as shown in Fig. 2(b). A slight reduction in the critical flux of 8.64 % was observed at an MLSS concentration of 18 g/L,

Table 3
Critical flux and critical time estimates.

Biomass concentration	Estimated parameters	No Sparging and Backwashing	Sparging Only	Backwashing Only	Combined Sparging and Backwashing
12 g/L	Critical Flux (LMH)	7.05	12.15	9.00	13.35
	Critical Time (min)	60.00	135.00	90.00	150.00
18 g/L	Critical Flux (LMH)	5.25	11.10	7.95	12.30
	Critical Time (min)	30.00	120.00	75.00	135.00
24 g/L	Critical Flux (LMH)	4.35	6.60	5.70	10.95
	Critical Time (min)	15.00	60.00	45.00	120.00

reaching 11.10 LMH. A significant reduction in critical flux was observed at an MLSS concentration of 24 g/L at a rate higher than 45 % and 40.54 % compared with MLSS of 12 and 18 g/L, respectively, as illustrated in Fig. 2(b). This indicates that biogas sparging can achieve higher flux rates even at moderately high biomass concentrations (MLSS $\leq$ 18 g/L) but could remain ineffective at significantly high MLSS concentrations [16]. Introducing biogas sparging helps disrupt the formation of a dense cake layer, which would otherwise lead to pore blocking and a decline in critical flux [39]. The study also revealed that the efficiency of sparging is negatively correlated with MLSS concentrations, while biogas sparging is much more effective at low biomass concentrations. At the same time, its effectiveness reduces at higher concentrations.

3.3. Impact of backwashing on critical flux

The experimental data analysis revealed insightful findings highlighting the influence of backwashing on the critical flux and fouling mitigation in a SAnMBR system. It was observed that at MLSS of 12 g/L, there was a 27.65 % increase in critical flux (9.0 LMH) compared to no biogas sparging or backwashing condition (7.05 LMH), as indicated in Fig. 2(c). Based on the results presented in Table 3, it was found that backwashing does not significantly improve the critical flux. As the MLSS concentration increased to 18 g/L, critical flux decreased by 11.66 %, attributing to 7.95 LMH with permeate backwashing. A further 28.30 % decrease in critical flux was observed at an MLSS concentration of 24 g/L, reaching 5.70 LMH while implementing permeate backwashing in the SAnMBR system. On the contrary, a notable increase in critical flux by 13.20 %, 52.88 %, and 31.03 % was observed while incorporating the backwashing strategy at MLSS of 12, 18, and 24 g/L, respectively, compared to no backwashing or biogas sparging condition, as shown in Table 3 and Fig. 2(a and c). This indicates that permeate backwashing offered some degree of fouling mitigation by removing organic foulants from the membrane surface, allowing permeability recovery [40]. This finding was consistent with the literature that the absence of any fouling control measures leads to severe membrane fouling affecting SAnMBR performance [41], while backwashing assists in attaining high flux rates. Compared to the backwashing-only condition with biogas sparging (Fig. 2(b) and (c)), the SAnMBR exhibited lower critical flux values across all MLSS concentrations. This indicates that SAnMBR operated with biogas sparging outperforms the backwashing technique in achieving higher critical flux rates across all biomass concentrations (12, 18, and 24 g/L), as shown in Table 3. For instance, at 12 g/L MLSS, the biogas sparging condition exhibits a 72.34 % increase in critical flux compared to the backwashing-only condition. Similarly, at 18 and 24 g/L MLSS concentrations, the SAnMBR system with only biogas sparging demonstrated a substantial increase in critical flux, approximately 111.43 % and 51.72 %, respectively, over the backwashing-only condition. This observation aligns with the research conducted by [42], who reported that sparging could effectively reduce membrane fouling and enhance the critical flux by up to 30 % compared to permeate backwashing. Furthermore, [43] and [44] investigated the influence of gas sparging and backwashing and found that backwashing was less effective than gas sparging in mitigating fouling and maintaining high flux rates. In summary, the comparison between the backwashing-only and sparging-only conditions at various MLSS concentrations highlights the effectiveness of biogas sparging in achieving higher critical flux values.

3.4. Impact of combined biogas sparging and backwashing on critical flux

The results show that the combined sparging and backwashing condition consistently shows the highest critical flux values across all biomass concentrations (12, 18, and 24 g/L) compared to the other conditions (no biogas sparging or backwashing, biogas sparging only, and backwashing only), as shown in Table 3 and Fig. 2(d). Wang, Jin [15] found that the combination of sparging and backwashing reduces fouling and improves critical flux values compared to individual sparging or backwashing techniques. The superior performance of the combined sparging and backwashing condition can be attributed to the complementary effects of both sparging and backwashing on fouling mitigation [10,45]. Sparging enhances turbulence and shear at the membrane surface, reducing cake layer formation and pore blocking, while backwashing provides intermittent cleaning, removing accumulated particles from the membrane surface [9,46,47]. This synergistic approach helps reduce pore blocking and maintain high flux rates, reducing filtration resistance.

In summary, the results and supporting literature indicate that the combined sparging and backwashing condition consistently yields the highest critical flux values at various MLSS concentrations compared to the other conditions. This combination significantly improves fouling control and demonstrates its potential as a practical approach to optimize membrane filtration processes. However, the cost-benefit aspects of the combined approach must be explored to evaluate the economic feasibility.

3.5. Unveiling the critical time influences on the critical flux

The critical time to reach critical flux is influenced by several factors [13,48]. Until now, only a few researchers have systematically researched the concept of critical time due to considerable gaps in understanding the concept and how it could influence the operational efficiency of the SAnMBR system. The influence of MLSS concentrations and the implementation of various fouling mitigation strategies to achieve a higher critical time are discussed comprehensively in the following subsections.

3.5.1. Influence of critical time on SAnMBR operation

While it may seem technically feasible to conclude that a process is more effective with a significantly high critical flux, this is not entirely accurate until both the critical flux and critical time are determined. On analysing the results in terms of critical time (min) for a biomass concentration of 12 g/L under conditions: no sparging and backwashing, sparging only, backwashing only, and combined sparging and backwashing, it becomes evident that the critical time varies significantly across the different conditions as shown in Table 3 and Figs. 3–5. The

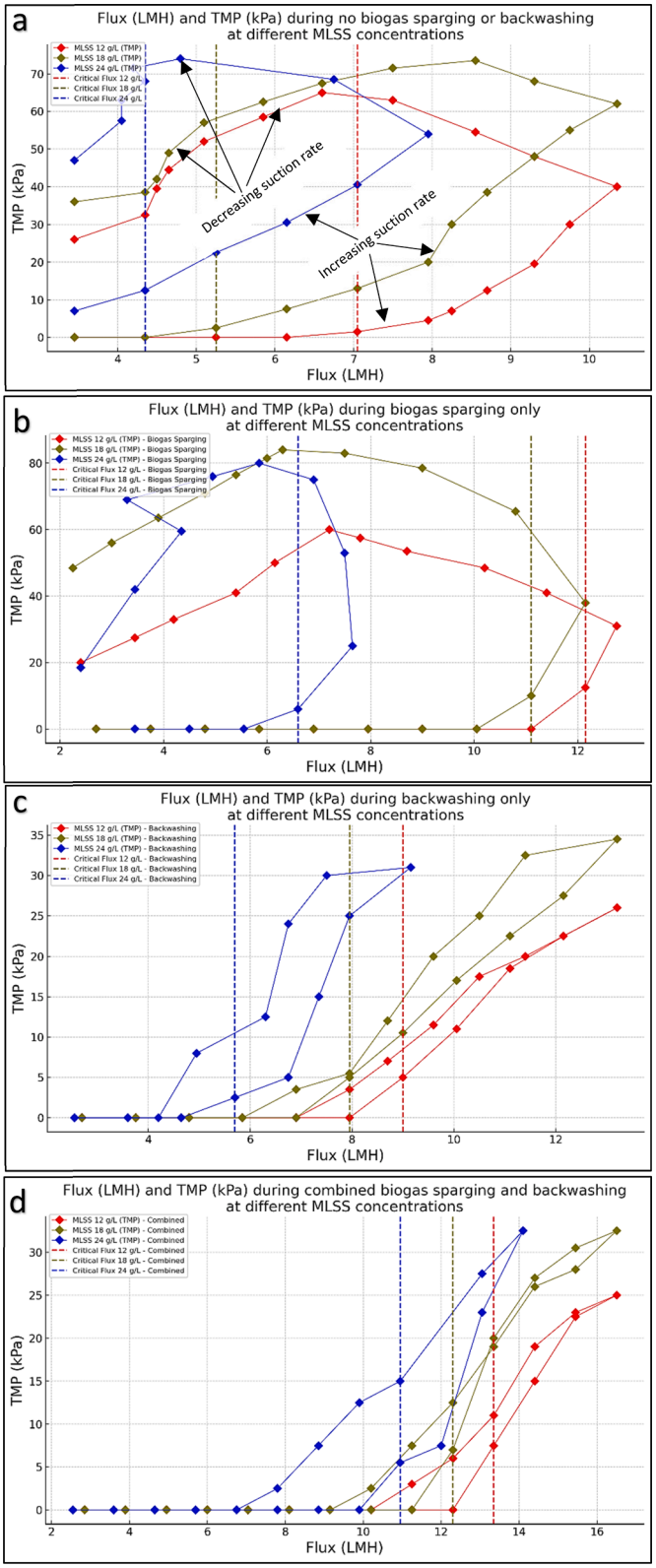

Fig. 2. Variation of TMP and flux at 12, 18 and 24 g/L for a) No backwashing or biogas sparging, b) Biogas sparging only, c) Backwashing only, d) Combined biogas sparging and backwashing.

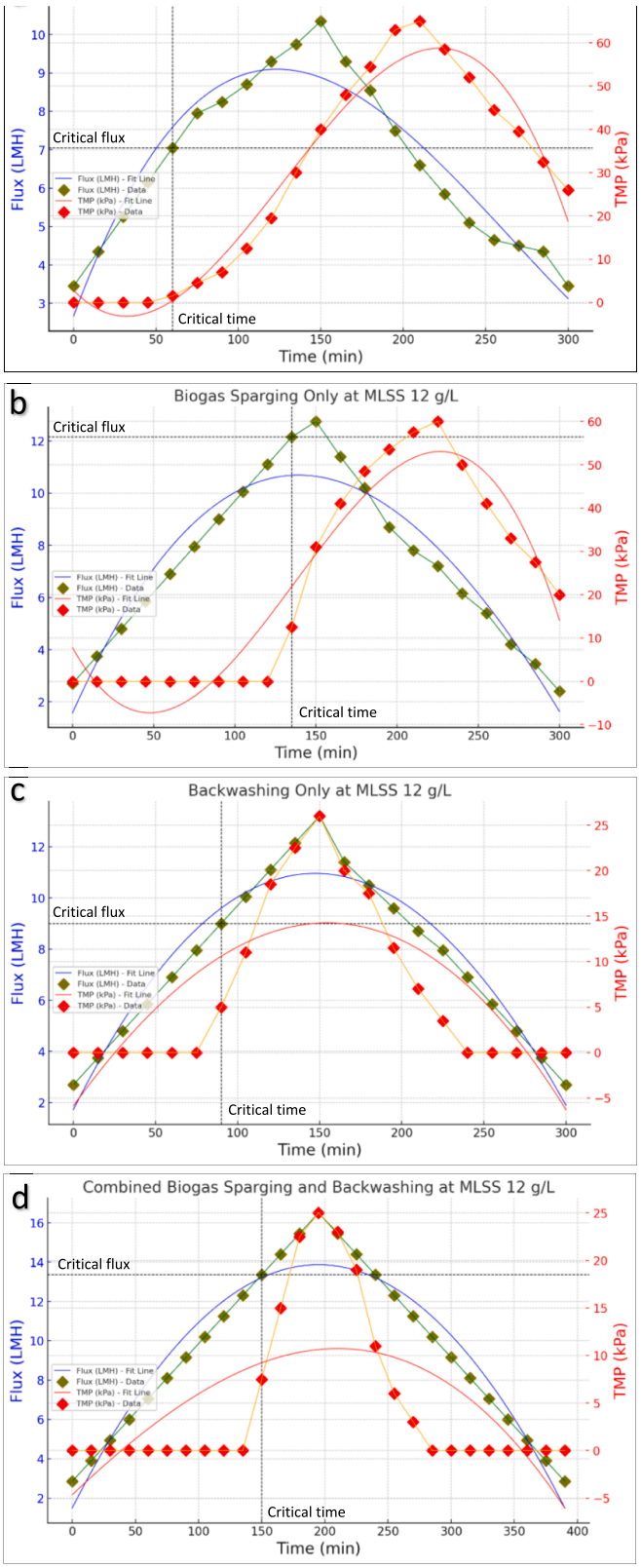

Fig. 3. Variation of flux and TMP vs time during critical flux test (CFT) conducted at 12 g/L for a) No backwashing or biogas sparging, b) Biogas sparging only, c) Backwashing only, d) Combined biogas sparging and backwashing.

combined sparging and backwashing condition in the SAnMBR system demonstrated the longest critical time of 150 min, followed by the sparging-only condition with a critical time of 135 min at MLSS of 12 g/L. The backwashing-only condition shows a critical time of 90 min,

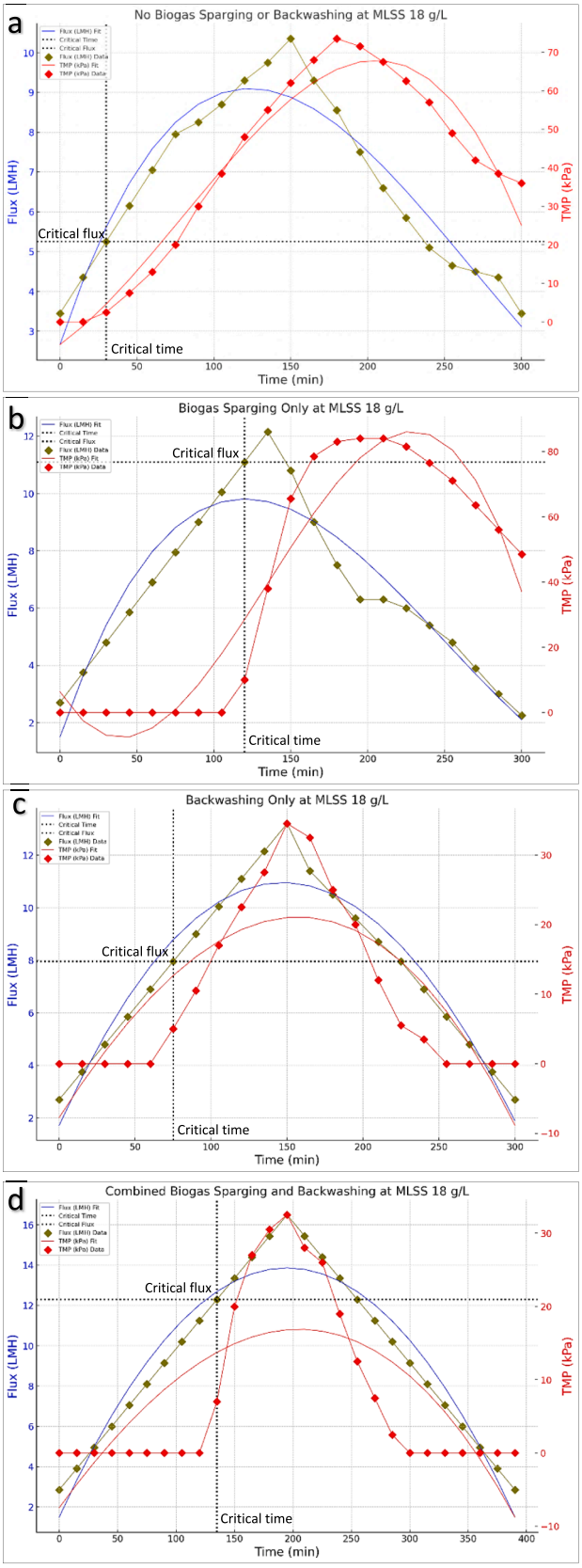

Fig. 4. Variation of flux and TMP vs time during critical flux test (CFT) conducted at 18 g/L for a) No backwashing or biogas sparging, b) Biogas sparging only, c) Backwashing only, d) Combined biogas sparging and backwashing.

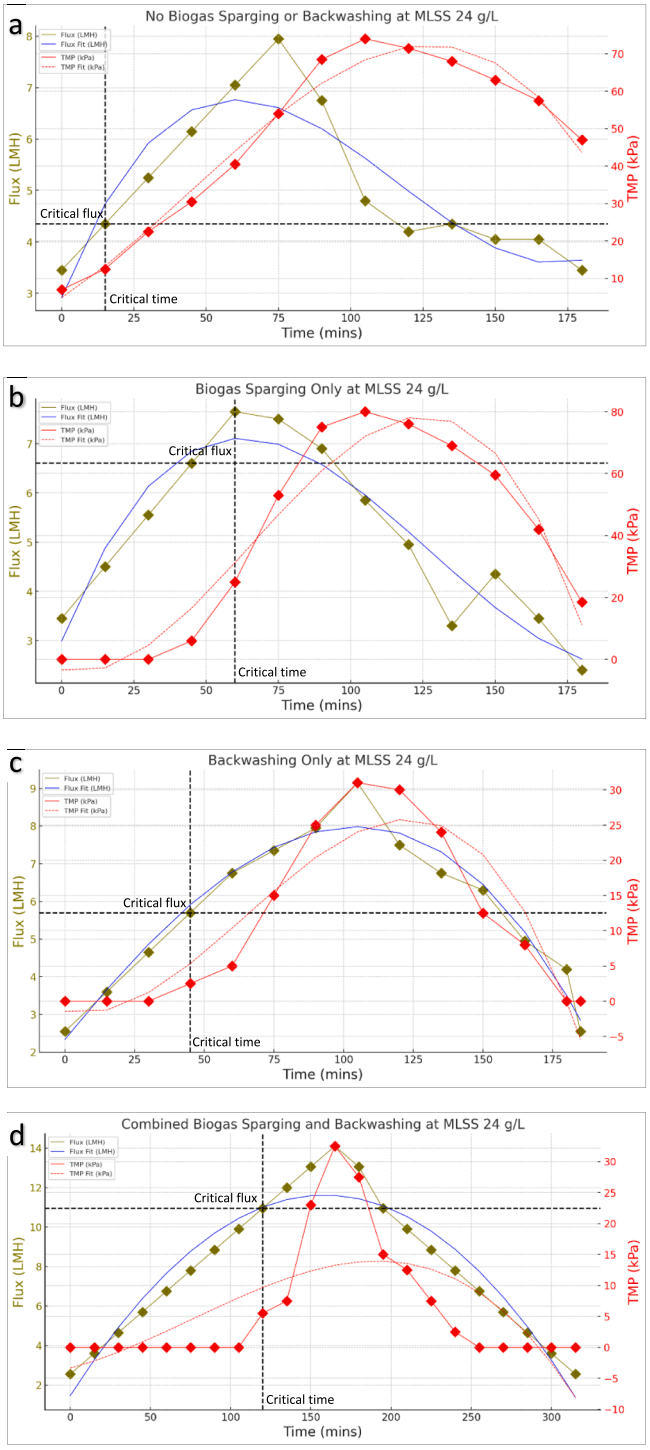

Fig. 5. Variation of flux and TMP vs time during critical flux test (CFT) conducted at 24 g/L for a) No backwashing or biogas sparging, b) Biogas sparging only, c) Backwashing only, d) Combined biogas sparging and backwashing.

while the no sparging and backwashing condition has the shortest critical time of 60 min, as shown in Fig. 3. Past research supports the trend observed in this study. For example, Charfi, Ben Amar [49] investigated the impact of combined sparging and backwashing in membrane fouling control and found that the combined approach significantly prolonged the critical time compared to individual sparging or backwashing strategies.

The critical time showed a decreasing trend when comparing the 12 g/L MLSS concentration values with those at 18 g/L for all conditions, as

shown in Fig. 4(a–d). The result shows that the critical time decreased by approximately 50 % (no sparging and backwashing), 11.11 % (sparging only), 16.67 % (backwashing only), and 10 % (combined sparging and backwashing) when the MLSS concentration is increased from 12 g/L to 18 g/L as shown in Table 3. However, as the biomass concentration increased to 24 g/L, the critical time decreased significantly for all conditions except for the combined conditions, as shown in Table 3 and Fig. 5. At MLSS of 24 g/L, the critical time was found to be shortest for the no sparging and backwashing condition (15 min), with a 50 % and 75 % decrease when compared with MLSS of 12 and 18 g/L, respectively, as shown in Table 3. The sparging-only condition, although found effective for fouling mitigation at MLSS concentrations of 12 and 18 g/L, was found ineffective with a significant decrease in critical time by 55.55 % and 50 %, respectively, reaching 60 min at 24 g/L as shown in Figs. 3–5(b). This could be attributed to inefficient scouring while using gas sparging at higher MLSS concentrations. A similar trend was observed while incorporating the backwashing-only condition at 24 g/L, as shown in Figs. 3–5(c), which led to a decrease in critical time to 45 min. This shows that the backwashing-only condition could not remove foulants from the pores and surface of the membrane even at moderately high MLSS of 18 g/L and above.

On the contrary, biogas sparging maintained a higher critical flux and time at 18 g/L concentration (11.10 LMH and 120 min). Among all conditions during the SAnMBR operation at 24 g/L, a lengthier critical time (120 min) was achieved using combined sparging and backwashing conditions, which can be attributed to the enhanced fouling control achieved through the synergistic effects of both biogas sparging and backwashing. This combination ensures a more sustained and efficient permeate flow, leading to a longer critical time before the membrane requires chemical cleaning. This highlights the potential of integrating sparging and backwashing to mitigate membrane fouling in SAnMBR systems operating under fluctuating biomass concentrations and ensuring longer intervals between cleaning cycles, leading to enhanced operational efficiency and reduced maintenance costs.

3.6. Fouling model simulation and interpretations

3.6.1. No backwashing and biogas sparging condition

Eqs. (3), (4), (6), (7), and (13) were simulated using the fixed parameter values taken from the literature, as shown in Table 2. Analyzing simulated results of membrane effective pore radius (m) and membrane resistance (1/m) for different biomass concentrations reveals complex trends for SAnMBR operation with no sparging or backwashing condition, as shown in Fig. 6 (a). At 12 g/L, the pore radius decreased gradually from 3.7×10^{-9} m to 2.0×10^{-9} m, characterized by a less steep slope, indicating a slower fouling rate and less pore blockage. The corresponding membrane resistance (1/m) increased from 1.5×10^{14} 1/m to 5.1×10^{14} 1/m, reflecting a steady buildup. At the onset of the filtration process, it was observed that internal fouling was predominant, which agreed with the findings reported by [50]. At 18 g/L, the pore radius decreased more pronouncedly from 3.7×10^{-9} m to 1.2×10^{-9} m, with a steeper slope, signifying moderate fouling propensity, while the membrane resistance increased from 1.6×10^{14} 1/m to 1.4×10^{15} 1/m, indicating a more significant obstruction to flow. At 24 g/L, with the pore radius decreasing sharply from 3.7×10^{-9} m to 2.2×10^{-9} m, reflecting the rapid fouling, with a high increase in resistance from 1.5×10^{14} 1/m to 4.4×10^{14} 1/m, denoting the most rapid buildup across all biomass concentrations. These findings agreed with [51] that higher biomass concentrations rapidly reduce the membrane's pore size and increase resistance without backwashing or gas-sparging strategies. The pore radius decreases sharply with higher MLSS concentrations, presumably due to an increased fouling rate and, eventually, pore blockage.

3.6.2. With biogas sparging only

The sparging condition consistently demonstrated a slower decrease

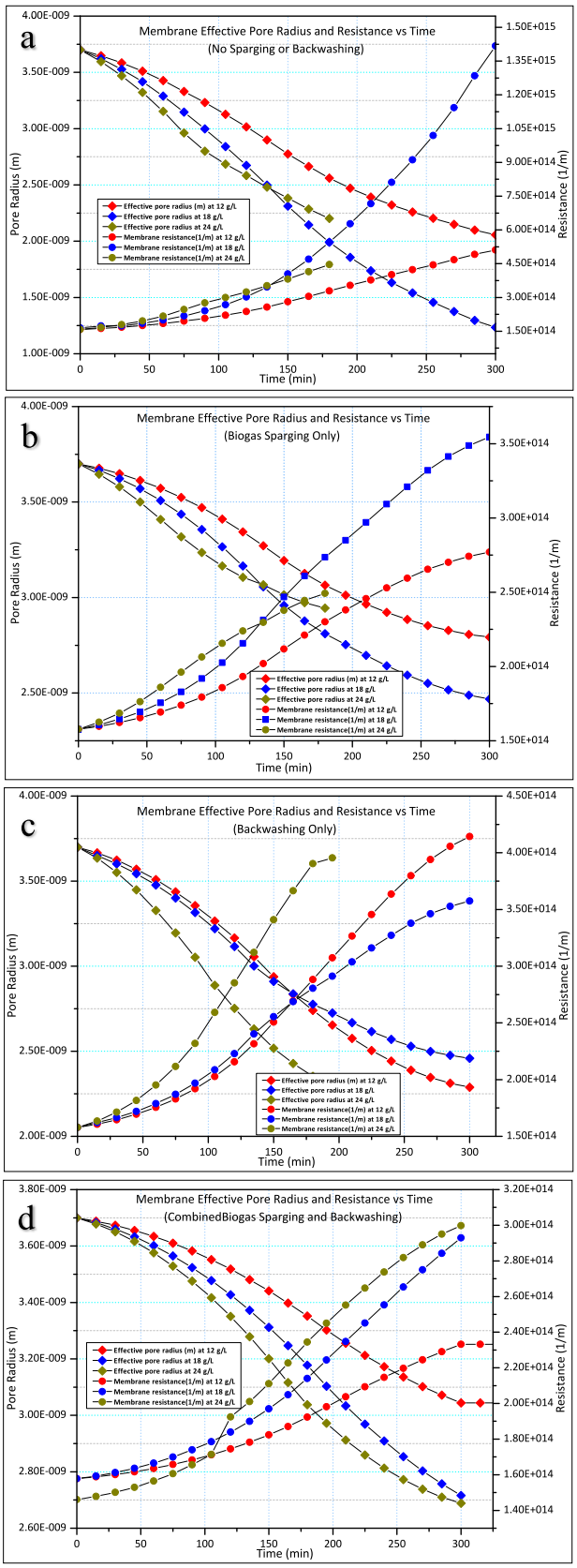

Fig. 6. Model simulation results for membrane resistance (1/m) and membrane effective pore radius (m) for a) no sparging or backwashing condition, b) biogas sparging only, c) backwashing only, and d) combined biogas sparging and backwashing at MLSS concentration of 12, 18, and 24 g/L.

in the effective pore radius (m) compared to no backwashing or biogas sparging condition across all biomass conditions. The membrane effective pore radius (m) decreased with corresponding increases in membrane resistance (1/m) from 1.5×10^{14} to 2.7×10^{14} 1/m, 3.5×10^{14} 1/m, and 2.49×10^{14} 1/m at 12, 18, and 24 g/L, respectively. The membrane effective pore radius decreases from 3.7×10^{-9} to 2.7×10^{-9} m, 2.8×10^{-9} m, and 2.9×10^{-9} m for MLSS concentrations of 12, 18, and 24 g/L, respectively. Biogas Sparging maintained a higher effective pore radius (m) at 12, 18, and 24 g/L, which remained at 2.7×10^{-9} m, 2.8×10^{-9} m, and 2.9×10^{-9} m compared to 2.2×10^{-9} m, 1.9×10^{-9} m, and 2.0×10^{-9} m for no backwashing or biogas sparging condition respectively. The effective pore radius (m) and membrane resistance (1/m) slope were less steep during biogas sparging conditions compared to no backwashing or sparging conditions, as shown in Fig. 6(b), demonstrating a better fouling control. As indicated by [9], biogas sparging reduces the coefficient of fouling, which increases the performance of SAnMBR, leading to cake layer reduction.

Technically, sparging reduces pore narrowing and the formation of a cake layer [15]. This can be justified by the hydrodynamic impact of sparging, which causes shear at the membrane surface. This shear effectively impedes the deposition and accumulation of particles on the membrane, thereby reducing the pore blockage and constriction rate [16]. In summary, this study affirms the fouling behaviour's complexity, where higher biomass concentrations lead to increased solute concentration polarization and cake layer formation. Although biogas sparging assisted in mitigating the fouling of the membrane at 12 g/L, the membrane resistance was still higher at 18 and 24 g/L, indicating the implementation of combination strategies or further optimization.

3.6.3. With backwashing only

Fig. 6(c) illustrates the impact of backwashing on the effective membrane pore radius (m) and membrane resistance (1/m) at MLSS concentrations of 12, 18, and 24 g/L. During the backwashing-only condition, the effective pore radius decreased from 3.7×10^{-9} m to 2.3×10^{-9} m at 12 g/L. This decrease was higher than the biogas sparging-only condition across all biomass concentrations. Concurrently, the membrane resistance increased from 1.5×10^{14} 1/m to 4.1×10^{14} 1/m for the 12 g/L scenario. The negative slope in pore radius and the positive slope in resistance became steeper with higher concentrations, signifying a more rapid change. Specifically, the 24 g/L scenarios showed the most pronounced changes, as shown in Fig. 6(c), consistent with higher concentrations leading to more substantial fouling effects.

Fig. 6(c) illustrates the trends in membrane-effective pore radius (m) and resistance (1/m). It shows that the area under the curve for pore radius (m) decreases with increasing biomass concentration, representing a progressive decrease in membrane-effective pore radius (m). In contrast, the corresponding area for membrane resistance (1/m) increases, reflecting cumulative growth over time. The negative slope for membrane-effective pore radius (m) increases with higher biomass concentrations, indicating a more rapid decrease in membrane pore size (m). Conversely, the positive slope for membrane resistance (1/m) becomes steeper, signifying a quicker increase with higher biomass concentrations [52]. Overall, the biogas sparging-only was more effective in mitigating fouling than backwashing-only conditions.

3.6.4. Combined biogas sparging and backwashing

Fig. 6(d) demonstrates that the pore radius (m) decreased linearly while the membrane resistance (1/m) increased linearly during continuous sparging and backwashing at MLSS concentrations of 12, 18, and 24 g/L. Specifically, for 12 g/L, the membrane effective pore radius (m) declines from 3.7×10^{-9} m to 3.0×10^{-9} m over time, and resistance grows from 1.5×10^{14} 1/m to 2.3×10^{14} 1/m. Similarly, for 18 g/L, the pore radius decreases from 3.7×10^{-9} to 2.7×10^{-9} m, and resistance increases from 1.5×10^{14} 1/m to 2.9×10^{14} 1/m. At MLSS of 24 g/L, the pore radius reduces from 3.7×10^{-9} m to 2.6×10^{-9} m, and resistance reaches 3.0×10^{14} 1/m from 1.4×10^{14} 1/m over the same duration. The membrane resistance slopes became steeper with increasing MLSS concentrations, as shown in Fig. 6(d), indicating the rate of increase in the membrane resistance (1/m). The trends show a more controlled decrease in pore radius (m) and a slower increase in membrane resistance (1/m) than backwashing-only, emphasizing the beneficial effect of continuous sparging on fouling mitigation. A more gradual and linear trend during combined biogas sparging and backwashing conditions reflects a more effective fouling control mechanism [53]. Higher biomass concentrations lead to a more significant increase in filtration resistance, which can be controlled using the combination of sparging and backwashing by enhancing mass transfer [9]. The scouring effect of gas bubbles reduces the thickness of the concentration polarization layer, while the hydrodynamics of backwashing, dependent on factors like flow rate and duration, can disrupt the cake layers [54], thereby achieving a high degree of SAnMBR performance. Overall, it was found that combining biogas sparging with backwashing presents a more feasible approach to maintaining higher critical flux rates and prolonged critical time in a SAnMBR system at higher biomass concentrations.

3.6.5. Estimation of critical parameters governing the fouling behaviour of the SAnMBR system

The model parameters, r (m), f (%), R_m (1/m), α_f (m^2/mg), and α_p (m^3/mg), were estimated from simulated and experimental data fitting results and summarised in Table 4. The parameters were compared to the baseline reference values of the new membrane obtained during the clean water flux test. It was found that the membrane effective pore radius *(r)* decreased by 21.67 % at MLSS of 12 g/L compared to the baseline value of 3.60×10^{-9} m (clean water) without biogas sparging and backwashing. Implementing fouling mitigation strategies, such as sparging or backwashing, alleviated the reduction, maintaining a higher *r*. The combined biogas sparging and backwashing condition led to an insignificant decrease in *r* by 7.78 %, sustaining the highest pore radius *(r)* of 3.32×10^{-9} m. The combined biogas sparging and backwashing condition at 24 g/L demonstrated its effectiveness, with only a 13.33 % reduction in *r*. The membrane resistance *(R_m)* increased by 92.77 % at MLSS of 12 g/L compared to the baseline value of 1.66×10^{14} (1/m) without backwashing or biogas sparging. This increase was significant at MLSS of 18 and 24 g/L, contributing to a sharp increase of 99.28 % and 233.13 % in the absence of any fouling mitigation strategies. On implementing biogas sparging, the increase in R_m was only 28.92 %, 22.89 %, and 50 % at MLSS of 12, 18, and 24 g/L, attributing to 2.14×10^{14}, 2.04×10^{14}, and 2.49×10^{14} (1/m), respectively, showing that biogas sparging is effective in mitigating fouling to a greater extent compared to the backwashing-only condition. The combined biogas sparging and backwashing were able to control the spike in R_m, limiting its increase by 19.28 %, 33.13 % and 40.36 % only at MLSS of 12, 18, and 24 g/L, respectively, as shown in Table 4. This finding agreed with studies conducted by [55,56].

The membrane porosity decrease *(f)* was microscopic due to the nature of this short-term experiment, with the highest decrease in porosity in the absence of fouling mitigation strategies (0.21– 0.29 %). However, a detailed microscopic comparative analysis shows that the decrease in porosity was highest in the absence of these fouling mitigation strategies (0.21 – 0.29 %), followed by the backwashing-only condition (0.13 – 0.16 %) at MLSS of 12, 18, and 24 g/L. This shows that combined conditions and biogas sparging alone could assist in maintaining an effective porosity in the membrane for its sustainable operation [48]. Backwashing, however, effectively mitigates fouling at low biomass concentrations and becomes ineffective at high biomass concentrations [8]. Other parameters, α_f (membrane porosity reduction coefficient) (m^2/mg), and α_p (membrane pore reduction coefficient) (m^3/mg) showed a similar trend at all biomass concentrations and were consistent with *r* and *f* values across all fouling mitigation strategies as shown in Table 4.

Table 4
Model estimated parameters.

Estimated parameters	Clean Water Flux Test (New Membrane)	MLSS 12 g/L				MLSS 18 g/L				MLSS 24 g/L			
		No Sparging and Backwashing	Sparging Only	Backwashing Only	Combined Sparging and Backwashing	No Sparging and Backwashing	Sparging Only	Backwashing Only	Combined Sparging and Backwashing	No Sparging and Backwashing	Sparging Only	Backwashing Only	Combined Sparging and Backwashing
r (m)	3.60×10^{-9}	2.82×10^{-9}	3.22×10^{-9}	2.97×10^{-9}	3.32×10^{-9}	2.89×10^{-9}	3.28×10^{-9}	2.75×10^{-9}	3.16×10^{-9}	2.39×10^{-9}	3.03×10^{-9}	3.00×10^{-9}	3.12×10^{-9}
f (%)	3.4978	3.4991	3.4995	3.4941	3.4996	3.4963	3.4995	3.4991	3.4995	3.4897	3.4993	3.4989	3.4994
R_m (1/m)	1.66×10^{14}	3.20×10^{14}	2.14×10^{14}	2.66×10^{14}	1.98×10^{14}	2.81×10^{14}	2.04×10^{14}	3.10×10^{14}	2.21×10^{14}	5.53×10^{14}	2.49×10^{14}	2.54×10^{14}	2.33×10^{14}
α_f (m^2/mg)	–	4x10^{-9}	2×10^{-9}	3×10^{-9}	1×10^{-9}	4x10^{-9}	2×10^{-9}	3×10^{-9}	1×10^{-9}	4x10^{-9}	2×10^{-9}	3×10^{-9}	1×10^{-9}
α_p (m^3/mg)	–	4x10^{-9}	2×10^{-9}	3×10^{-9}	1×10^{-9}	4x10^{-9}	2×10^{-9}	3×10^{-9}	1×10^{-9}	4x10^{-9}	2×10^{-9}	3×10^{-9}	1×10^{-9}

r is membrane effective pore radius (m), *f* is the decrease in membrane porosity (%), *Rm* is the membrane resistance (1/m), α_f is membrane porosity reduction coefficient (m^2/mg), α_p is membrane pore reduction coefficient (m^3/mg).

3.7. Membrane morphological analysis using SEM-EDX spectroscopy

The morphology and chemical composition of the ceramic UF membrane was investigated using SEM-EDX spectroscopic. The formation of cake layers was insignificant while operating the SAnMBR system at an MLSS of 12 g/L. The scanning electron microscopy (SEM) images of the new membrane (Fig. 7(a and b)) exhibit a uniformly even surface. In contrast, the fouled membrane displayed a comparatively uneven surface and appeared to contain clusters of particulate matter that could include bacterial cells, as depicted in Fig. 7(f). The expedition of the cake layer on the membrane surface could be attributed to the hydrophobic nature of EPS, which was found to be the primary constituent of the cake layer [8]. It can be seen from Fig. 7(d and f) that cake-layer formation was significant during the CFT conducted at 18 and 24 g/L. Due to the consolidation of EPS at the cake layer during CFT at 24 g/L, visible cracks in the cake layer can be seen in Fig. 7(f). The membrane pores were readily apparent in the cross-sectional analysis of the clean and fouled membranes, as depicted in Fig. 7(a and c) at MLSS of 12 and 18 g/L. However, a significant pore blockage could be seen in the membrane cross-section during CFT conducted at 24 g/L (Fig. 7(e)), meaning pore blockage was significant at high-biomass concentration. This finding agreed with the experimental and modelling results of this study. The study revealed that under extreme biomass concentrations (>18 g/L), the conventional backwashing and gas sparging method was ineffective in removing the cake layer and pore blockage.

Considering the elemental analysis the fingerprint of the membrane composition (Al_2O_3) was responsible for the significant peaks of Al and O that were detected in a high concentration in all the samples Fig. 7(a – f). The elevated concentration of Carbon (C) on the membrane surface (34.04 % and 52.74 %) during CFT at 18 and 24 g/L (Fig. 7(d and f)), respectively, indicates that organic fouling increased at higher biomass concentrations. On the contrary, a low concentration of C in the membrane cross-section (10.82 % and 11.93 %) was seen during CFT at 18 and 24 g/L, indicating that organic fouling inside the membrane pores was insignificant, as shown in Fig. 7(c and e). While a relatively high concentration of Ca (10.80 %), Phosphorus (P) (6.43 %), Sodium (Na) (0.78 %), and Mn (0.25 %) were detected in the membrane pores at a high-biomass concentration (24 g/L), indicating pore-blocking phenomenon due to elevated concentrations of inorganic foulants. This summarises that backwashing or gas sparging helped mitigate fouling at low and moderate biomass concentrations while inadequate for mitigating pore-blocking at high biomass concentrations.

3.8. Sludge composition analysis using proton Nuclear Magnetic Resonance (NMR) spectroscopy

The NMR spectroscopic analysis provided a more comprehensive understanding of the chemical composition of the sludge of the SAnMBR bioreactor. The chemical shifts for hydrogens in carbohydrates and proteins exhibit characteristic ranges reflective of their specific chemical environments. As depicted in Fig. S2(a, b, and c), the NMR spectra demonstrate a wide range of organics in all three samples, suggesting a complex composition of extracellular polymeric substances (EPS) in the reactors. Anomeric hydrogens of sugars in EPS polysaccharides appeared in the region of 4.5 to 5.5 ppm, while proteinaceous components correspond with the aliphatic region (0.5 to 4.0 ppm) [57] and aromatic region (6.5 to 8.5 ppm) [34] as shown in Fig. S2(a, b, and c). These findings can be attributed to the existence of humic-like substances and proteins or free amino acids, respectively [58]. This observation indicates that the SAnMBR exhibited a higher concentration of polysaccharides and lipids at a higher biomass (MLSS > 18 g/L) concentration, as shown in Fig. S2(b and c), which supported cake formation and pore-blocking due to EPS.

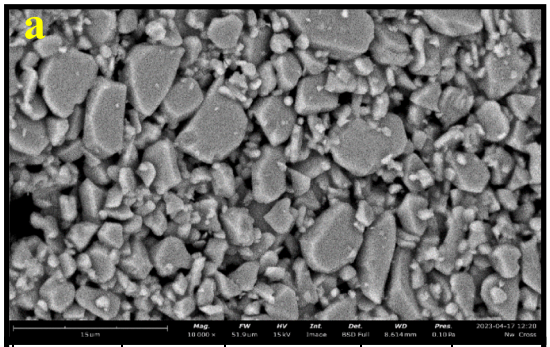

Element Number	Element Symbol	Element Name	Atomic Conc.	Weight Conc.
6	C	Carbon	5.609	3.504
8	O	Oxygen	63.396	52.753
9	F	Fluorine	0.304	0.300
13	Al	Aluminum	30.616	42.943

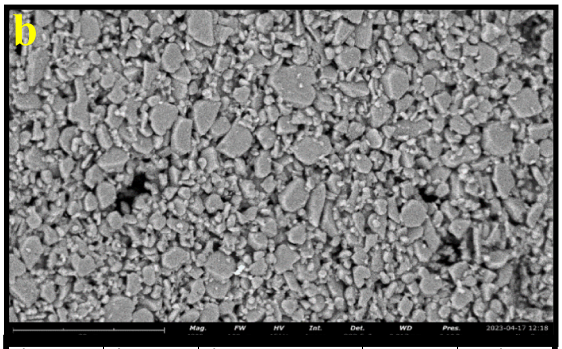

Element Number	Element Symbol	Element Name	Atomic Conc.	Weight Conc.
6	C	Carbon	6.367	3.700
8	O	Oxygen	49.473	38.300
13	Al	Aluminum	41.994	54.800
14	Si	Silicon	2.134	2.900

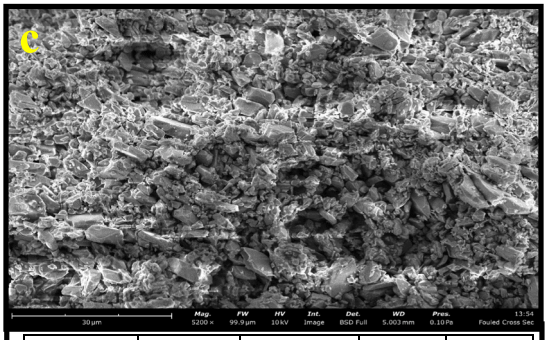

Element Number	Element Symbol	Element Name	Atomic Conc.	Weight Conc.
6	C	Carbon	10.862	6.400
8	O	Oxygen	47.647	37.400
9	F	Fluorine	0.000	0.000
13	Al	Aluminum	40.132	53.100
14	Si	Silicon	0.943	1.300

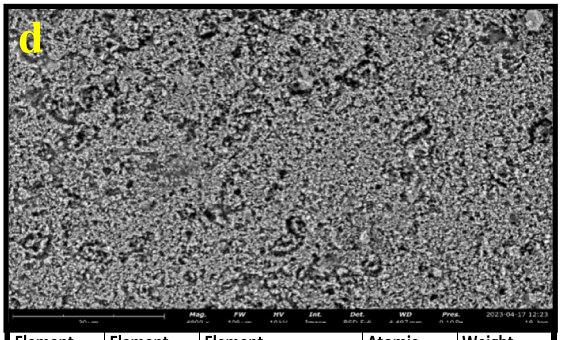

Element Number	Element Symbol	Element Name	Atomic Conc.	Weight Conc.
6	C	Carbon	34.049	21.831
8	O	Oxygen	33.685	28.773
13	Al	Aluminum	28.927	41.650
14	Si	Silicon	1.610	2.414
17	Cl	Chlorine	0.531	1.006
20	Ca	Calcium	0.987	2.113

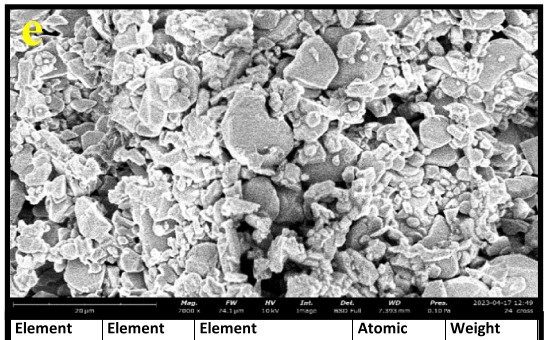

Element Number	Element Symbol	Element Name	Atomic Conc.	Weight Conc.
6	C	Carbon	11.903	7.100
8	O	Oxygen	65.563	52.100
9	F	Fluorine	0.424	0.400
11	Na	Sodium	0.788	0.900
12	Mg	Magnesium	0.828	1.000
13	Al	Aluminum	2.538	3.400
15	P	Phosphorus	6.434	9.900
20	Ca	Calcium	10.801	21.500
25	Mn	Manganese	0.257	0.700

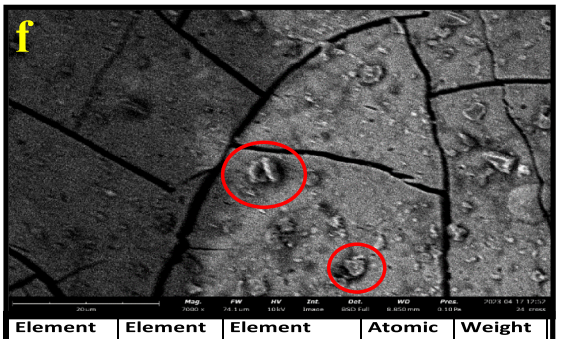

Element Number	Element Symbol	Element Name	Atomic Conc.	Weight Conc.
6	C	Carbon	52.740	41.200
8	O	Oxygen	36.513	38.000
9	F	Fluorine	1.133	1.400
13	Al	Aluminum	9.007	15.800
25	Mn	Manganese	0.028	0.100
26	Fe	Iron	0.083	0.300

Fig. 7. SEM-EDX spectroscopy of (a) Cross-section of new membrane, (b) Longitudinal section of new membrane, (c) Cross-section of the fouled membrane at MLSS 18 g/L, (d) Longitudinal section of the fouled membrane at MLSS 18 g/L, (e) Cross-section of the fouled membrane at MLSS 24, (f) Longitudinal section of the fouled membrane at MLSS 24 g/L.

3.9. Statistical analysis and data validation

A linear and polynomial model of degree three was fitted with the experimental results to identify the onset of fouling and critical points (critical flux and time). From the results, the polynomial regression model captured the data trend better than the linear regression model and fitted well with experimental data, providing a more reasonable estimate for the critical values (critical flux and time). This finding agreed with previous studies [27,29,31]. The mean absolute error (MAE) values for the polynomial model were consistently lower than the linear model, indicating better accuracy of the polynomial model [30]. At the same time, the mean squared error (MSE) values for the polynomial model were lower than the linear model, further confirming the superiority of the polynomial model [29], as shown in Table 5. The R^2 value of fitted data using the polynomial model was found in the range > 0.90, significantly higher than the linear model, showing a significant fit as shown in Table 5. As discussed in S.3 (Supplementary information), a heat map was generated to represent the correlation matrix visually, illustrating the relationships between flux (LMH) and transmembrane pressure (TMP) across various conditions and MLSS concentrations (Fig. S3).

4. Conclusion

The extensive investigation into the key operating parameters, effective fouling mitigation strategies, and flux performance under various biomass concentrations has provided substantial insights for operating the SAnMBR system sustainably. The key findings of this study are:

- At MLSS of 12 g/L, the pore radius decreased by 21.67 % in the absence of mitigation strategies but implementing biogas sparging and backwashing maintained higher pore radius of 3.22×10^{-9} and 2.97×10^{-9} m, respectively. Combining both strategies resulted in only a 7.78 % decrease in pore radius (3.32×10^{-9} m).
- At MLSS of 18 g/L, the pore radius decreased more pronouncedly from 3.7×10^{-9} m to 1.2×10^{-9} m, signifying moderate fouling propensity, while the membrane resistance increased from 1.6×10^{14} 1/m to 1.4×10^{15} 1/m, indicating a more significant obstruction to flow.
- At MLSS of 24 g/L, there was a 33.61 % decrease in the pore radius in the absence of backwashing or sparging strategies, resulting in the smallest pore radius (2.39×10^{-9} m), but combining both strategies resulted in only a 3.33 % decrease in pore radius. Membrane resistance increased by 92.77 % at 12 g/L MLSS compared to baseline (1.66×10^{14} 1/m) without mitigation strategies and by 99.28 % and 233.13 % at 18 and 24 g/L, respectively.
- On implementing biogas sparging, the increase in R_m was only 28.92 %, 22.89 %, and 50 % at MLSS of 12, 18, and 24 g/L, attributing to 2.14×10^{14}, 2.04×10^{14}, and 2.49×10^{14} (1/m), respectively, showing that biogas sparging is effective in mitigating fouling to a greater extent compared to the backwashing strategy.
- The combined backwashing and biogas sparging outperformed the individual fouling mitigation strategy, achieving the highest critical flux rates and time across all biomass concentrations.
- The membrane porosity decrease (f) was microscopic. However, a detailed microscopic comparative analysis shows that the decrease in porosity was highest in the absence of these fouling mitigation strategies (0.21——0.29 %), followed by the backwashing strategy (0.13——0.16 %) at MLSS of 12, 18, and 24 g/L.
- SEM-EDX analysis further provided insights into membrane morphology, revealing significant pore blocking at high biomass concentrations (>18 g/L) due to EPS and inorganic foulants, while the NMR analysis confirmed the presence of EPS in the bioreactor's sludge.

In summary, the ceramic UF membrane coupled with the SAnMBR system could be operated at high-biomass concentration ranges (up to 18 g/L) with biogas sparging and backwashing at a critical flux of 12.30 LMH, leading to efficient and sustainable membrane filtration processes. The study also highlights potential directions for further research into varying MLSS concentrations or exploring other membrane types, which could further refine these fouling mitigation strategies. Future research should also focus on understanding the influence of microbial secretion on the critical flux and membrane fouling and using a comprehensive microbiological investigation.

CRediT authorship contribution statement

Rajneesh Kumar Gautam: Writing – original draft, Visualization, Validation, Software, Project administration, Methodology, Investigation, Formal analysis, Data curation, Conceptualization. **Akangbe Olubukola:** Writing – original draft, Visualization, Validation, Methodology, Formal analysis. **Saumya Verma:** Writing – review & editing, Visualization, Validation, Software, Formal analysis. **Shobha Muthukumaran:** Writing – review & editing, Supervision, Project administration. **Dimuth Navaratna:** Writing – review & editing, Supervision, Project administration, Methodology, Investigation, Conceptualization.

Declaration of competing interest

The authors declare that they have no known competing financial interests or personal relationships that could have appeared to influence the work reported in this paper.

Table 5
Statistical analysis of the experimental data for each condition of the study.

MLSS 12 g/L	Critical Flux (J_c)	Slope	Polynomial MAE	Linear MAE	Polynomial MSE	Linear MSE	Polynomial R^2	Linear R^2
No Biogas Sparging or Backwashing	7.05	0.739	0.4964	1.8155	0.3395	4.3735	0.9251	0.0353
Biogas Sparging Only	12.15	0.013	0.7371	2.6367	0.7510	9.5320	0.9218	0.0071
Backwashing Only	9.00	0.443	0.6399	2.6667	0.6238	9.5716	0.9348	0.0001
Combined Biogas Sparging and Backwashing	13.35	−0.135	0.8725	3.5490	1.0706	16.7901	0.9362	0.0000
MLSS 18 g/L								
No Biogas Sparging or Backwashing	5.25	1.033	2.37	8.64	13.04	156.45	0.940	0.253
Biogas Sparging Only	11.10	0.150	4.40	9.98	48.36	225.05	0.907	0.347
Backwashing Only	7.95	0.600	3.31	6.53	24.08	74.55	0.797	0.00059
Combined Biogas Sparging and Backwashing	12.30	−0.006	4.01	6.68	33.82	73.75	0.714	0.00039
MLSS 24 g/L								
No Biogas Sparging or Backwashing	4.35	1.187	0.510	1.071	0.37	1.78	0.911	0.091
Biogas Sparging Only	6.60	0.811	0.449	1.266	0.26	2.26	0.903	0.172
Backwashing Only	5.70	0.957	0.311	1.678	0.19	3.80	0.952	0.008
Combined Biogas Sparging and Backwashing	10.95	0.170	0.828	2.968	0.98	12.02	0.918	0.000

*MAE- Mean absolute error, MSE- Mean square error.

Data availability

Data will be made available on request.

Appendix A. Supplementary data

Supplementary data to this article can be found online at https://doi.org/10.1016/j.cej.2024.151972.

References

[1] J. Ji, et al., Submerged anaerobic membrane bioreactor applied for mainstream municipal wastewater treatment at a low temperature: Sludge yield, energy balance and membrane filtration behaviors, J. Clean. Prod. 355 (2022) 131831.
[2] Q. Sohaib, et al., Fouling and clogging behavior of porous membrane during biogas recovery from submerged granular anaerobic membrane bioreactor permeate; long-term stability analysis, J. Water Process Eng. 53 (2023) 103717.
[3] S. Saha, et al., An integrated leachate bed reactor – anaerobic membrane bioreactor system (LBR-AnMBR) for food waste stabilization and biogas recovery, Chemosphere 311 (2023) 137054.
[4] S.M.A. Abuabdou, et al., A review of anaerobic membrane bioreactors (AnMBR) for the treatment of highly contaminated landfill leachate and biogas production: Effectiveness, limitations and future perspectives, J. Clean. Prod. 255 (2020) 120215.
[5] M.T. Vu, et al., A hybrid anaerobic and microalgal membrane reactor for energy and microalgal biomass production from wastewater, Environ. Technol. Innov. 19 (2020) 100834.
[6] H.J. Lin, et al., Sludge properties and their effects on membrane fouling in submerged anaerobic membrane bioreactors (SAnMBRs), Water Res 43 (15) (2009) 3827–3837.
[7] L. Dvořák, et al., Anaerobic membrane bioreactors—a mini review with emphasis on industrial wastewater treatment: applications, limitations and perspectives, Desalin. Water Treat. 57 (41) (2015) 19062–19076.
[8] G. Balcıoğlu, G. Yilmaz, Z.B. Gönder, Evaluation of anaerobic membrane bioreactor (AnMBR) treating confectionery wastewater at long-term operation under different organic loading rates: Performance and membrane fouling, Chem. Eng. J. 404 (2021) 126261.
[9] A. Olubukola, et al., Development of a dynamic model for effective mitigation of membrane fouling through biogas sparging in submerged anaerobic membrane bioreactors (SAnMBRs), J Environ Manage 323 (2022) 116151.
[10] R.K. Gautam, et al., Evaluation of long-term operational and treatment performance of a high-biomass submerged anaerobic membrane bioreactor treating abattoir wastewater, Chem. Eng. J. (2023) 142145.
[11] C.S. Laspidou, B.E. Rittmann, A unified theory for extracellular polymeric substances, soluble microbial products, and active and inert biomass, Water Res 36 (11) (2002) 2711–2720.
[12] B. Benyahia, et al., Anaerobic membrane bioreactor modeling in the presence of Soluble Microbial Products (SMP) – the Anaerobic Model AM2b, Chem. Eng. J. 228 (2013) 1011–1022.
[13] H. Cheng, et al., Enhancement of sustainable flux by optimizing filtration mode of a high-solid anaerobic membrane bioreactor during long-term continuous treatment of food waste, Water Res 168 (2020) 115195.
[14] A.D. Grossman, et al., Effect of ultrafiltration membrane material on fouling dynamics in a submerged anaerobic membrane bioreactor treating domestic wastewater, Environ. Sci. Water Res. Technol. 5 (6) (2019) 1145–1156.
[15] T. Wang, et al., In-depth insights into the temporal-based fouling mechanism and its exploration in anaerobic membrane bioreactors: A review, J. Clean. Prod. 375 (2022) 134110.
[16] R.A. Fox, D.C. Stuckey, The effect of sparging rate on transmembrane pressure and critical flux in an AnMBR, J Environ Manage 151 (2015) 280–285.
[17] D. Navaratna, V. Jegatheesan, Implications of short and long term critical flux experiments for laboratory-scale MBR operations, Bioresour Technol 102 (9) (2011) 5361–5369.
[18] Judd, S., The MBR book: principles and applications of membrane bioreactors for water and wastewater treatment. 2010: Elsevier.
[19] L. Gutu, et al., Multi-Integrated Systems for Treatment of Abattoir Wastewater: A Review, Water 13 (18) (2021) 2462.
[20] P.W. Harris, B.K. McCabe, Process Optimisation of Anaerobic Digestion Treating High-Strength Wastewater in the Australian Red Meat Processing Industry, Appl. Sci. 10 (2020), https://doi.org/10.3390/app10217947.
[21] Z. Wang, et al., Membrane cleaning in membrane bioreactors: a review, J. Membr. Sci. 468 (2014) 276–307.
[22] R.K. Gautam, et al., Recovery of biomethane from a submerged anaerobic membrane bioreactor treating domestic wastewater blended with semi-solid organic wastes discharged from residential establishments, Environ. Technol. Innov. 27 (2022) 102763.
[23] P. Le Clech, et al., Critical flux determination by the flux-step method in a submerged membrane bioreactor, J. Membr. Sci. 227 (1–2) (2003) 81–93.
[24] P. Bacchin, P. Aimar, R.W. Field, Critical and sustainable fluxes: Theory, experiments and applications, J. Membr. Sci. 281 (1–2) (2006) 42–69.
[25] C. Psoch, S. Schiewer, Long-term flux improvement by air sparging and backflushing for a membrane bioreactor, and modeling permeability decline, Desalination 230 (1–3) (2008) 193–204.
[26] P. Le-Clech, V. Chen, T.A. Fane, Fouling in membrane bioreactors used in wastewater treatment, J. Membr. Sci. 284 (1–2) (2006) 17–53.
[27] S. Park, et al., Enhancement of operating flux in a membrane bio-reactor coupled with a mechanical sieve unit, Chemosphere 191 (2018) 573–579.
[28] S. Ognier, C. Wisniewski, A. Grasmick, Membrane bioreactor fouling in sub-critical filtration conditions: a local critical flux concept, J. Membr. Sci. 229 (1–2) (2004) 171–177.
[29] M. Cifuentes-Cabezas, et al., Deep Study on Fouling Modelling of Ultrafiltration Membranes Used for OMW Treatment: Comparison Between Semi-empirical Models, Response Surface, and Artificial Neural Networks, Food Bioproc. Tech. (2023) 1–21.
[30] A. Reyhani, et al., Application of evolutionary polynomial regression in ultrafiltration systems considering the effect of different parameters on oily wastewater treatment, J. Pet. Sci. Technol. 3 (1) (2013) 9.
[31] A. Klimkiewicz, A.E. Cervera-Padrell, F. van den Berg, Modeling of the flux decline in a continuous ultrafiltration system with multiblock partial least squares, Ind. Eng. Chem. Res. 55 (40) (2016) 10690–10698.
[32] E.W. Rice, L. Bridgewater, A.P.H. Association, Standard Methods for the Examination of Water and Wastewater, Vol. 10, American public health association Washington, DC, 2012.
[33] W.E. Federation, A. Association, Standard methods for the examination of water and wastewater, American Public Health Association (APHA), Washington, DC, USA, 2005.
[34] S. Shakeri Yekta, et al., Molecular characterization of particulate organic matter in full scale anaerobic digesters: An NMR spectroscopy study, Sci. Total Environ. 685 (2019) 1107–1115.
[35] Giraldo, E. and M. LeChevallier. Dynamic mathematical modeling of membrane fouling in submerged membrane bioreactors. in WEFTEC 2006. 2006. Water Environment Federation.
[36] S. Lee, et al., The effect of floc size and structure on specific cake resistance and compressibility in dead-end microfiltration, Sep. Sci. Technol. 38 (4) (2003) 869–887.
[37] C.-S. Tran, et al., Anaerobic baffled reactor coupled with membrane bioreactor treating tannery wastewater, Case Studies in Chemical and Environmental Engineering 5 (2022) 100185.
[38] E. Yuliwati, et al., Critical Flux and Fouling Analysis of PVDF-Mixed Matrix Membranes for Reclamation of Refinery-Produced Wastewater: Effect of Mixed Liquor Suspended Solids Concentration and Aeration, Membranes 12 (2) (2022) 161.
[39] M. Aslan, et al., Effect of biogas sparging with different membrane modules on membrane fouling in anaerobic submerged membrane bioreactor (AnSMBR), Environ Sci Pollut Res Int 21 (5) (2014) 3285–3293.
[40] I. Ruigómez, et al., Evaluation of a novel physical cleaning strategy based on HF membrane rotation during the backwashing/relaxation phases for anaerobic submerged MBR, J. Membr. Sci. 526 (2017) 181–190.
[41] Y. Cheng, H. Li, Rheological behavior of sewage sludge with high solid content, Water Sci Technol 71 (11) (2015) 1686–1693.
[42] E.B. Estrada-Arriaga, P. Mijaylova Nacheva, L. García-Sánchez, Effect of mixed liquor volatile suspended solids on membrane fouling during short and long-term operation of membrane bioreactor. Ingeniería y, Ciencia 11 (21) (2015) 137–155.
[43] J. Wu, C. He, Y. Zhang, Modeling membrane fouling in a submerged membrane bioreactor by considering the role of solid, colloidal and soluble components, J. Membr. Sci. 397 (2012) 102–111.
[44] S. Delgado, R. Villarroel, E. González, Effect of the shear intensity on fouling in submerged membrane bioreactor for wastewater treatment, J. Membr. Sci. 311 (1–2) (2008) 173–181.
[45] B.D. Shoener, et al., Energy positive domestic wastewater treatment: the roles of anaerobic and phototrophic technologies, Environ Sci Process Impacts 16 (6) (2014) 1204–1222.
[46] M.E. Ersahin, et al., Gas-lift anaerobic dynamic membrane bioreactors for high strength synthetic wastewater treatment: Effect of biogas sparging velocity and HRT on treatment performance, Chem. Eng. J. 305 (2016) 46–53.
[47] Z. Liu, et al., Quantitative relationships for the impact of gas sparging conditions on membrane fouling in anaerobic membrane bioreactor, J. Clean. Prod. (2020) 123139.
[48] Y. Jang, et al., Investigation of critical sludge characteristics for membrane fouling in a submerged membrane bioreactor: Role of soluble microbial products and extracted extracellular polymeric substances, Chemosphere 271 (2021) 129879.
[49] A. Charfi, N. Ben Amar, J. Harmand, Analysis of fouling mechanisms in anaerobic membrane bioreactors, Water Res 46 (8) (2012) 2637–2650.
[50] J. Liang, L. Yu, J. Wu, The dynamic change of specific cake resistance in membrane bioreactor due to periodical cake relaxation, J. Environ. Chem. Eng. 8 (4) (2020) 103837.
[51] D.-W. Gao, et al., Membrane fouling in an anaerobic membrane bioreactor: Differences in relative abundance of bacterial species in the membrane foulant layer and in suspension, J. Membr. Sci. 364 (1–2) (2010) 331–338.
[52] M. Turker, R.K. Dereli, Long term performance of a pilot scale anaerobic membrane bioreactor treating beet molasses based industrial wastewater, J Environ Manage 278 (Pt 1) (2021) 111403.
[53] N.S.A. Mutamim, Z.Z. Noor, Assessment of Membrane Bioreactor in Treating Spent Sulfidic Caustic Wastewater: Effects of Organic Biomass Concentration and Solid Retention Time, Chem. Eng. Res. Bull. 19 (2017) 102–110.
[54] A. Charfi, et al., A modelling approach to study the fouling of an anaerobic membrane bioreactor for industrial wastewater treatment, Bioresour Technol 245 (Pt A) (2017) 207–215.

[55] J. Ji, et al., One-year operation of a 20-L submerged anaerobic membrane bioreactor for real domestic wastewater treatment at room temperature: Pursuing the optimal HRT and sustainable flux, Sci Total Environ 775 (2021) 145799.
[56] Y. Hu, et al., A review on anaerobic membrane bioreactors for enhanced valorization of urban organic wastes: Achievements, limitations, energy balance and future perspectives, Sci. Total Environ. 820 (2022) 153284.
[57] F. Meng, et al., Characterization of the size-fractionated biomacromolecules: tracking their role and fate in a membrane bioreactor, Water Res. 45 (15) (2011) 4661–4671.
[58] K. Kimura, et al., Membrane fouling in pilot-scale membrane bioreactors (MBRs) treating municipal wastewater, Environ. Sci. Tech. 39 (16) (2005) 6293–6299.
[59] A. Charfi, et al., A modelling approach to study the fouling of an anaerobic membrane bioreactor for industrial wastewater treatment, Bioresour Technol 245 (Pt A) (2017) 207–215.
[60] T. Toshinori, N. Shin-ichi, K. Shoji, Effective charge density and pore structure of charged ultrafiltration membrane, J. Chem. Eng. Jpn. 23 (5) (1990) 604–610.
[61] A. Olubukola, et al., Development of a dynamic model for effective mitigation of membrane fouling through biogas sparging in submerged anaerobic membrane bioreactors (SAnMBRs), J Environ Manage 323 (2022).
[62] N.L. Tanko, The effect of Porosity on Tortuosity, IJSER 9 (2018) 2163–2169.
[63] R.K. Gautam, et al., Evaluation of membrane cake fouling mechanism to estimate design parameters of a submerged AnMBR treating high strength industrial wastewater, J Environ Manage 301 (2022).